Mon. Not. R. Astron. Soc. **326,** 1391–1402 (2001)

The binary fraction of extreme horizontal branch stars

P. F. L. Maxted,[1,2★] U. Heber,[3] T. R. Marsh[1] and R. C. North[1]

[1]*University of Southampton, Department of Physics & Astronomy, Highfield, Southampton, S017 1BJ*
[2]*Department of Physics, Keele University, Staffordshire, ST5 5BG*
[3]*Dr. Remeis-Sternwarte, Astronomisches Institut der Universität Erlangen-Nürnberg, Sternwartstrasse 7, 96049 Bamberg, Germany*

Accepted 2001 May 18. Received 2001 March 26; in original form 2000 December 12

ABSTRACT

We have used precise radial velocity measurements of subdwarf-B stars from the Palomar–Green catalogue to look for binary extreme horizontal branch (EHB) stars. We have determined the effective temperature, surface gravity and surface helium abundance for 20 of the targets from new or existing blue spectra and have compiled published values for these quantities for all but one other. We identify 36 EHB stars in our sample and find that at least 21 of these stars are binaries. All but one or two of these are new identifications. The minimum binary fraction for EHB stars implied by our survey is 60 ± 8 per cent. Our survey is sensitive to binaries with orbital periods $P \lesssim 10$ d. For reasonable assumptions concerning the period distribution and the mass ratio distribution of the binaries, we find that the mean detection efficiency of our survey over this range of orbital periods is 87 per cent. Allowing for this estimated detection efficiency, the fraction of EHB stars that are short-period binaries ($0.03\,\mathrm{d} \lesssim P \lesssim 10\,\mathrm{d}$) is 69 ± 9 per cent. The value is not strongly dependent on the period distribution below $P \approx 10$ d or the mean companion mass for these short-period binaries. The orbital separation of the stars in these binaries is much less than the size of the red giant from which the EHB star has formed. This is strong evidence that binary star evolution is fundamental to the formation of the majority of EHB stars. If there are also binary EHB stars, the orbital periods of which are $\gtrsim$10 d, the fraction of EHB stars for which evolution was affected by the presence of a companion may be much higher, e.g. if one third of EHB stars are binaries with orbital periods $10\,\mathrm{d} \lesssim P \lesssim 100\,\mathrm{d}$, then our observations are consistent with all EHB stars being formed through some type of binary star evolution. We find that five of the other stars we observed are likely to be post-EHB stars, one of which is also a binary.

Key words: binaries: close – binaries: spectroscopic – subdwarfs.

1 INTRODUCTION

Surveys for blue stars brighter than $B \approx 16$ are dominated by subdwarf-B (sdB) stars (Green, Schmidt & Liebert 1986). The effective temperatures ($T_{\rm eff}$) and surface gravities ($\log g$) of the majority of these stars place them on the extreme horizontal branch (EHB), i.e., they appear in the same region of the $T_{\rm eff}$–$\log g$ plane as evolutionary tracks for core helium-burning stars with core masses of about $0.5\,\mathrm{M}_\odot$ and extremely thin ($\lesssim 0.02\,\mathrm{M}_\odot$) hydrogen envelopes (Heber 1986; Saffer et al. 1994). We make a distinction in this paper between the nomenclature 'sdB star', which is a spectral classification, and 'EHB star' which is an interpretation of the evolutionary state of a star.

The observed dispersion of core masses for EHB stars is very low ($< 0.04\,\mathrm{M}_\odot$, Saffer et al. 1994). It is thought that the eventual fate of an EHB star is to cool to form a white dwarf with a mass of about $0.5\,\mathrm{M}_\odot$, which is low compared with the typical mass for white dwarfs (Bergeron, Saffer & Liebert 1992). The formation of low-mass white dwarfs is, in general, thought to involve interactions with a binary companion star, e.g. a common envelope phase, in which a companion to a red giant star is engulfed by the expanding outer layers. The resulting friction causes the companion to spiral in towards the core of the red giant, ejecting the envelope at the expense of orbital binding energy (Iben & Livio 1993). If this process occurs while the red giant is within ~ 0.4 mag of the tip of the red giant branch, the core can go on to ignite helium, despite the dramatic mass loss, and may then appear as an EHB star (D'Cruz et al. 1996; Mengel, Norris & Gross 1976).

The binary fraction of sdB and EHB stars is expected to be high given the scenario outlined above. Allard et al. (1994) found that 31 of their sample of 100 sdB stars show flat spectral energy distributions which indicate the presence of companions with spectral types in the range late G to early M. They infer a binary

★E-mail: pflm@astro.keele.ac.uk

fraction for main-sequence companions of 54–66 per cent, although the companions in their survey appear to be overluminous compared with normal main-sequence stars. A similar conclusion was reached by Ferguson, Green & Liebert (1984) using a similar argument and by Jeffery & Pollacco (1998) based on the detection of spectral features arising from cool companions. What is not clear from these observations is whether the cool companion is sufficiently close to the EHB star to be implicated in the mass loss process that is supposed to form the EHB star. These techniques are also insensitive to white dwarf companions and faint M-dwarf companions. Companions to EHB stars can also be detected in eclipsing systems such as the short-period EHB–M dwarf binaries HW Vir (Wood & Saffer 1999) and PG 1336−018 (Kilkenny et al. 1998) and in EHB–white dwarf binaries that show ellipsoidal variability, e.g. KPD 0422+5421 (Koen, Orosz & Wade 1998) and KPD 1930+2752 (Maxted, Marsh & North 2000b). These binaries are extremely useful for studying the properties of EHB stars, but they do not offer a useful method for finding binary EHB stars in general because the probability of such a binary showing eclipses or a measurable ellipsoidal effect decreases rapidly for increasing orbital periods.

Radial velocity surveys are an excellent method for identifying binary stars in general, particularly since the efficiency of this technique can be accurately quantified and the selection effects are well understood. This technique can be applied to many types of star, from main-sequence stars (Duquennoy & Mayor 1991) to white dwarfs (Maxted & Marsh 1999). For EHB stars in particular, this is the method of choice because the short-period binaries that are expected to result from a common-envelope phase are the easiest to identify using this method. If the radial velocities are measured to an precision of a few $\mathrm{km\,s^{-1}}$ and the observations are obtained over a baseline of weeks or months the technique has the potential to identify binaries with much longer periods ($\sim$100 d) even if the companion is a low mass M dwarf. Saffer, Livio & Yungelson (1998) have shown the potential for this technique with their observations of 46 sdB stars. The precision of their radial velocity measurements was modest (20–30 $\mathrm{km\,s^{-1}}$) and the three spectra they obtained for each star over a baseline of 1–2 d were compared by-eye, yet they found that at least seven of their sample of 46 sdB stars show radial velocity variations. Several of these binaries have subsequently had their orbital periods determined (Moran et al. 1999; Maxted et al. 2000a), although further observations are required to determine the nature of the companions in these binaries.

In this paper we present the results of a radial velocity survey of binary EHB stars. We have used observations of the Hα line to measure 205 precise radial velocities for 36 EHB stars from the Palomar–Green survey (Green et al. 1986). We positively identify 22 short-period binary EHB stars, 20 of which are new discoveries. We conclude that at least 60 ± 8 per cent of EHB stars are short-period binary stars. If we allow for the detection efficiency of our survey, we find that at least 69 ± 9 per cent of EHB stars are binaries. This is strong evidence that binary star evolution is fundamental to the formation of the majority of EHB stars. We also observed five stars which we identify as post-EHB stars and found that one of these stars is a binary.

2 OBSERVATIONS AND REDUCTIONS

2.1 Hα spectra

Targets were selected from objects in the Palomar–Green catalogue (Green et al. 1986) classified as sdB stars. We avoided stars where follow-up observations have shown that the classification was in error or that the star is not an EHB star. Observations were obtained with the 2.5-m Isaac Newton Telescope on the Island of La Palma. Spectra were obtained with the intermediate dispersion spectrograph using the 500-mm camera, a 1200 line $\mathrm{mm^{-1}}$ grating and a TEK charge-coupled device (CCD) as a detector. The spectra cover 400 Å around the Hα line at a dispersion of 0.39 Å per pixel. The slit width used was 0.97 arcsec which gave a resolution of about 0.9 Å. Spectra of the targets were generally obtained in pairs bracketed by observations of a copper-neon arc. We obtained a total of 243 spectra for 43 stars over a total of about seven nights during the interval 2000 April 10–21. The seeing was good ($\approx$1 arcsec) on most of these nights.

Extraction of the spectra from the images was performed automatically using optimal extraction to maximize the signal-to-noise ratio of the resulting spectra (Marsh 1989). The arcs associated with each stellar spectrum were extracted using the same weighting determined for the stellar image to avoid possible systematic errors resulting from the tilt of the spectra on the detector. The wavelength scale was determined from a fourth-order polynomial fit to measured arc line positions. The standard deviation of the fit to the 8 arc lines was typically 0.09 Å. The wavelength scale for an individual spectrum was determined by interpolation to the time of mid-exposure from the fits to arcs taken before and after the spectrum to account for the small amount of drift in the wavelength scale ($<$0.1 Å) arising from flexure of the instrument. Statistical errors on every data point calculated from photon statistics are rigorously propagated through every stage of the data reduction.

2.2 Blue spectra

In order to measure the effective temperature and surface gravity of some our targets we also obtained blue spectra of our targets with the same telescope and instrument. We did not attempt to measure radial velocities from these spectra.

Spectra of PG 1032+406, PG 1043+760, PG 1051+501, PG 1039+219, PG 1043+760 and PG 1110+294 were obtained over the wavelength range 3810–5020 Å using a 400 line $\mathrm{mm^{-1}}$ grating. The observations were obtained while the stars were at low airmass in good seeing with a vertical 1.5-arcsec slit. The resolution in pixels was determined from the width of the spatial profile, which was typically 3–4 pixels, which corresponding to a resolution of about 4 Å.

We used an EEV CCD on the 235-mm camera and a 900 line $\mathrm{mm^{-1}}$ grating to obtain spectra of PG 1505+074, 1512+244 and 1553+273 on the night 2000 July 16 and of PG 1616+144, 1627+017, 1632+088, 1647+056, and 1653+131 on the night 2000 August 15. The useful region of the spectra cover the wavelength range 3590–5365 Å at a dispersion of 0.63 Å per pixel. We used a vertical, 1 arcsec wide slit which gave a resolution of 1.6 Å. We also obtained spectra of PG 0907+123 and 1116+301 on the night of 2001 February 3 with the same instrument covering the wavelength range 3850–5200 Å. One other spectrum of PG 0907+123 was also obtained and reduced for us by Martin Altman using the Calar Alto 2.2-m telescope and the CAFOS spectrograph with a B100 grism at a dispersion of 100 Å $\mathrm{mm^{-1}}$ at lower spectral resolution than our INT spectra, but covering the Balmer lines from Hβ to H10.

3 ANALYSIS

3.1 Effective temperatures, surface gravities and helium abundances

For those stars for which we have blue spectra we measured the effective temperature, $T_{\rm eff}$, the surface gravity $\log g$ and the helium abundance by number, y. The simultaneous fitting of Balmer line profiles by a grid of synthetic spectra has become the standard technique to determine the atmospheric parameters of hot high-gravity stars (Bergeron et al. 1992). The procedure has been extended to include helium line profiles and applied successfully to sdB stars by Saffer et al. (1994). We have applied Saffer's procedure to the Balmer lines (Hβ to H 9), and the He I (4026, 4388, 4471, 4713, 4922 Å) and He II 4686 Å lines.

A grid of synthetic spectra derived from H and He line blanketed non-local thermodynamic equilibrium (NLTE) model atmospheres (Napiwotzki 1997) was matched to the data to determine simultaneously the effective temperature, surface gravity and helium abundance. For stars cooler than 27 000 K we used the metal line-blanketed local thermodynamic equilibrium (LTE) model atmospheres of Heber, Reid & Werner (2000). The synthetic spectra were convolved beforehand with a Gaussian profile of the appropriate width to account for the instrumental profile. The adopted values of $T_{\rm eff}$, $\log g$ and y for these stars and all other stars where values could be found are given in Table 1. Examples of the observed spectral lines and synthetic spectrum fits for six sdB stars are shown in Fig. 1. The values given for PG 1040+234 are only approximate because of the contamination by the companion star, particularly in the Hϵ line, which we excluded from the fit. The values given for PG 1701+359, 1722+286 and 1743+477 are based on updated fits to the spectra described by Theissen et al. (1993). The values for PG 0907+123 are an average of the values derived from our INT spectrum and the spectrum taken by Martin Altman, which agree very well.

The measured values of $T_{\rm eff}$ and $\log g$ are compared to the evolutionary tracks for extreme horizontal branch stars of Dorman, Rood & O'Connell (1993) in Fig. 2. It can be seen that most the targets lie in or near the band defined by the zero-age extreme horizontal branch (ZAEHB), the terminal-age extreme horizontal branch (TAEHB) and the helium main-sequence (HeMS) and are therefore EHB stars. The errors in the atmospheric parameters are estimated to be 3 per cent for $T_{\rm eff}$ and 0.1 dex for $\log g$ and the helium abundance y. We consider a star to be a post-EHB star if it lies above the TAEHB by more than these error bars, otherwise we regard it as an EHB star. The spectra of PG 1040+234 and 1701+359 are contaminated by the cool companion. The principal effect of this contamination is to bias the value of $\log g$ to lower values, so we treat the value obtained as an upper limit in Table 1 and in Fig. 2. Both these stars are included as EHB stars in our discussion of the binary fraction of EHB stars. PG 1632+088 is too cool to appear in Fig. 2. It is probably a normal horizontal branch star so we exclude it from our discussion of the binary fraction of EHB stars. We also exclude PG 0909+164, 1000+408, 1051+501, 1505+074 and 1553+273 because they lie too far from the EHB in the $T_{\rm eff}$–$\log g$ plane. They appear to be more evolved than EHB stars so we classify them as post-EHB stars and discuss them separately from the EHB stars. We also exclude PG 1631+267 from our discussion of the binary fraction of EHB stars because no $T_{\rm eff}$–$\log g$ measurement is available for this star.

Table 1. Measured values of $T_{\rm eff}$, $\log g$ and y from blue spectra for our targets. We also give the y magnitude in the Strömgren system, m_y, from Wesemael et al. (1992) and Bergeron et al. (1984). References are as follows: 0 This work; 1 Saffer et al. (1994); 2 Saffer, private communication; 3 Moehler et al. (1990); 4 O'Donoghue et al. (1998).

Name	m_y	$T_{\rm eff}$ (kK)	$\log g$ (cgs)	y	Ref.
PG 0749+658	12.14	24.6	5.54	0.004	1
PG 0839+399	14.39	36.1	5.91	0.002	1
PG 0849+319	14.61	28.9	5.37	0.003	2
PG 0850+170	13.98	27.1	5.37	0.006	2
PG 0907+123	13.97	26.2	5.30	0.018	0
PG 0909+164	13.85	35.4	5.64	0.002	2
PG 0918+029	13.42	31.7	6.03	0.008	1
PG 0919+273	12.77	31.9	5.97	0.011	1
PG 1000+408	13.33	36.4	5.54	0.002	2
PG 1017−086	14.43	30.2	5.62	0.003	2
PG 1018−047	13.32	31.0	5.75	0.002	2
PG 1032+406	11.52	31.6	5.77	0.005	0
PG 1039+219	13.09	33.1	5.64	0.007	0
PG 1040+234[a]	13.37	34.8	>5.26	>0.030	0
PG 1043+760	13.77	27.6	5.39	0.002	0
PG 1047+003	13.48	35.0	5.9		4
PG 1051+501	13.38	33.8	4.96	0.040	0
PG 1110+294	14.09	30.1	5.72	0.019	0
PG 1114+073	13.06	29.8	5.81	0.006	1
PG 1116+301	14.34	32.5	5.85	0.006	0
PG 1237+132	14.65	33.1	5.93	0.002	2
PG 1244+113	14.20	33.8	5.67	0.001	2
PG 1248+164	14.40[b]	26.6	5.68	0.001	2
PG 1300+279	14.27	29.6	5.65	0.005	2
PG 1303+097	14.50	30.3	5.76	0.011	2
PG 1329+159	13.55	29.1	5.62	0.004	2
PG 1417+257	13.78	27.6	5.43	0.005	2
PG 1505+074	12.44	37.1	5.42	0.0008	0
PG 1512+244	13.28	29.9	5.74	0.009	0
PG 1553+273	13.61	22.1	4.74	0.001	0
PG 1616+144	13.50	36.5	6.02	0.031	0
PG 1619+522	13.30	32.3	5.98	0.011	1
PG 1627+017	12.93	22.8	5.27	0.001	0
PG 1631+267	15.51				–
PG 1632+088	13.19	13.3	3.78	0.004	0
PG 1647+056	14.75	33.6	5.95	0.015	0
PG 1653+131	14.50	25.6	5.40	0.002	0
PG 1701+359[a]	13.22	31.4	>5.50	>0.0003	0
PG 1710+490	12.90	29.9	5.74	0.006	1
PG 1716+426	13.97	27.4	5.47	0.003	1
PG 1722+286	13.40	35.8	5.94	0.035	0
PG 1725+252	13.01	28.9	5.54	0.0009	0
PG 1743+477	13.79	25.5	5.41	0.007	0

[a] Spectrum contaminated by cool companion.
[b] Photographic magnitude.

3.2 Radial velocity measurements

To measure the radial velocities we used least-squares fitting of a model line profile. This model line profile is the summation of three Gaussian profiles with different widths and depths but with a common central position which varies between spectra. Only data within 2000 km s^{-1} of the Hα line is included in the fitting process and the spectra are normalized using a linear fit to the continuum either side of the Hα line.

To measure the radial velocities we use a fitting process with four steps to determine an optimum set of radial velocities. We use a least-squares fit to one of the spectra to determine an initial shape of the model line profile. A least squares fit of this profile to each spectrum in which the position of the line is the only free parameter gives an initial set of radial velocities. We use these initial radial

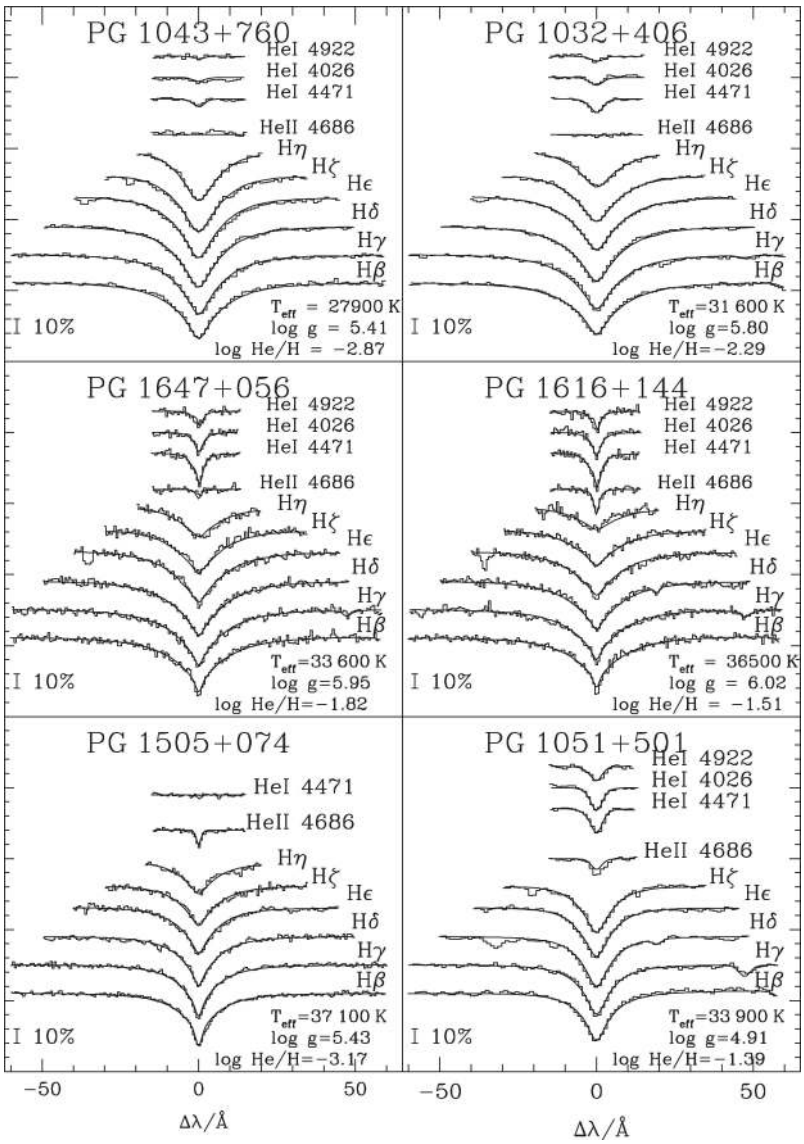

Figure 1. Examples of the observed spectral lines and synthetic spectrum fits for six sdB stars.

velocities to fix the position of the Hα line in a simultaneous fit to all the spectra to obtain an improved model line profile. A least-squares fit of this profile to each spectrum yields the radial velocities given in Table 2. The uncertainties quoted are calculated by propagating the uncertainties on every data point in the spectra right through the data reduction and analysis. These uncertainties are reliable in most cases, but some caution must be exercised for quoted uncertainties $\lesssim 2\,\mathrm{km\,s^{-1}}$. This corresponds to about 1/10 of a pixel in the original data, so systematic errors such as telluric absorption features, uncertainties in the wavelength calibration and motion of the star within the slit during good seeing are certain to be a significant source of uncertainty for these measurements. An example of the observed spectra and multiple Gaussian fits for one star is shown in Fig. 3.

We rebinned all the spectra on to a common wavelength scale allowing for the measured radial velocity shifts and then formed the average spectrum of each star shown in Fig. 4.

3.3 Criterion for variability

For each star we calculate a weighted mean radial velocity. This

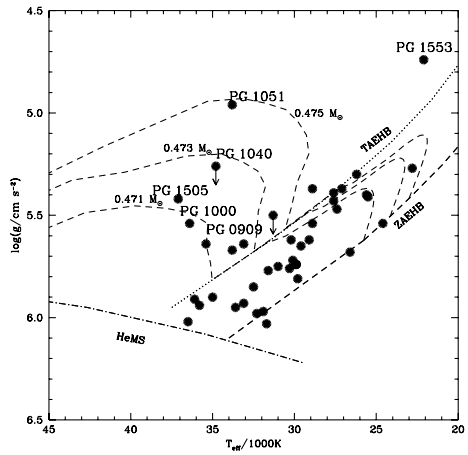

Figure 2. The measured values of $T_{\rm eff}$ and $\log g$ for our targets compared with the evolutionary models of Dorman et al. (1993). Evolutionary tracks are shown as dashed lines and are labelled with the mass of the helium core they refer to. The other symbols are defined in the text. Stars discussed in the text are labelled by the first six characters of their PG catalogue names. Small arrows denote measurements that are upper limits.

Table 2. Measured heliocentric radial velocities.

Name	HJD −2451600	Radial velocity (km s^{-1})
PG 0749+658		
	46.3402	−8.7 ± 3.9
	46.3412	−10.8 ± 4.3
	51.3388	−11.9 ± 2.4
	51.3405	−10.4 ± 2.2
	54.3339	5.7 ± 3.9
	54.3356	−0.7 ± 3.3
	56.3462	−10.9 ± 2.0
	56.3478	−11.5 ± 2.1
	57.3379	−4.0 ± 2.8
	57.3396	−6.1 ± 2.4
PG 0839+399		
	46.3498	52.4 ± 8.6
	46.3562	31.9 ± 8.8
	51.3528	64.7 ± 4.6
	51.3677	55.8 ± 4.3
	54.3695	−5.3 ± 5.1
	54.3820	−7.0 ± 4.8
PG 0849+319		
	46.3657	93.0 ± 4.3
	46.3733	82.0 ± 4.3
	51.3816	119.3 ± 4.1
	51.3891	127.6 ± 4.1
PG 0850+170		
	46.4208	69.2 ± 1.8
	46.4333	66.3 ± 1.9
	54.3966	27.0 ± 2.2
	54.4067	25.2 ± 2.0
PG 0907+123		
	47.4116	87.3 ± 2.7
	47.4323	83.2 ± 2.2
	53.3980	101.1 ± 4.0
	53.4084	92.6 ± 6.7
	54.4213	34.9 ± 3.4
	54.4351	37.8 ± 1.9
PG 0909+164		
	47.4525	59.4 ± 6.5
	47.4677	42.6 ± 6.9
	53.3753	43.4 ± 5.4
	53.3856	52.0 ± 5.5
	56.3918	51.4 ± 5.5
	56.4021	48.8 ± 5.4
	57.3921	68.3 ± 5.1
	57.4024	57.4 ± 5.2
PG 0918+029		
	47.4808	35.0 ± 5.9
	47.4861	26.1 ± 11.0
	53.3633	95.0 ± 5.0
	53.3669	107.4 ± 4.5
PG 0919+273		
	53.3518	−77.2 ± 4.1
	53.3562	−83.3 ± 3.8
	54.4461	−57.5 ± 3.2
	54.4505	−58.3 ± 3.2

Table 2 – *continued*

Name	HJD −2451600	Radial velocity (km s^{-1})
PG 1000+408		
	49.3644	66.4 ± 11.4
	49.3687	76.4 ± 9.4
	51.3991	102.6 ± 4.2
	51.4054	95.6 ± 4.1
	51.4197	91.7 ± 4.5
	51.4260	83.9 ± 4.3
	56.3593	85.4 ± 4.9
	56.3661	102.0 ± 4.9
	57.3492	77.8 ± 4.4
	57.3575	84.7 ± 3.8
PG 1017−086		
	46.4502	−66.2 ± 7.1
	46.4614	−4.5 ± 6.4
PG 1018−047		
	46.4713	33.5 ± 3.8
	46.4765	21.7 ± 3.7
	54.4607	24.8 ± 3.2
	54.4678	33.0 ± 3.2
	56.4141	27.6 ± 4.0
	56.4192	29.1 ± 4.0
	57.4141	15.8 ± 4.1
	57.4192	24.5 ± 4.0
PG 1032+406		
	49.3760	−8.6 ± 4.2
	49.3777	−15.3 ± 3.4
	51.4124	23.1 ± 2.4
	51.4141	22.5 ± 2.4
PG 1039+219		
	53.4438	0.4 ± 2.9
	53.4500	−2.5 ± 2.9
	56.4266	−7.5 ± 3.3
	56.4330	−7.6 ± 3.0
	57.4266	−3.5 ± 3.0
	57.4328	0.8 ± 2.9
PG 1040+234		
	53.4582	11.5 ± 2.6
	53.4641	8.1 ± 2.8
	54.4761	9.7 ± 2.2
	54.4821	8.4 ± 2.2
	56.4411	11.0 ± 2.5
	56.4471	12.6 ± 2.4
	57.4406	7.4 ± 2.4
	57.4466	9.1 ± 2.4
PG 1043+760		
	49.3849	−28.1 ± 3.2
	49.3959	−3.8 ± 3.3
	51.4332	−21.7 ± 3.1
	51.4402	−5.8 ± 3.1
PG 1047+003		
	53.4284	−3.2 ± 5.0
	53.4357	−0.0 ± 5.1
	56.4560	−1.7 ± 5.2
	56.4617	−11.1 ± 5.1
	57.4579	−9.8 ± 3.8

Table 2 – *continued*

Name	HJD −2451600	Radial velocity (km s^{-1})
	57.4690	−12.9 ± 3.8
PG 1051+501		
	53.5281	−133.8 ± 4.7
	53.5355	−127.5 ± 5.0
	56.3752	−126.8 ± 5.8
	56.3811	−128.9 ± 5.6
	57.3692	−124.7 ± 3.4
	57.3796	−130.3 ± 3.3
PG 1110+294		
	53.4747	11.1 ± 11.9
	53.4845	14.1 ± 9.1
	56.5069	−0.6 ± 2.6
	56.5167	−0.3 ± 2.6
	57.4808	−39.3 ± 2.8
	57.4906	−40.8 ± 2.8
PG 1114+073		
	47.5230	8.6 ± 2.6
	47.5338	7.7 ± 2.4
	54.5177	5.7 ± 1.5
	54.5259	11.3 ± 1.5
	56.4693	12.0 ± 2.0
	56.4749	8.5 ± 1.9
	57.5014	9.5 ± 2.0
	57.5070	8.6 ± 2.0
PG 1116+301		
	53.5014	−89.4 ± 3.8
	53.5164	−86.4 ± 2.7
	56.5285	82.5 ± 2.8
	56.5386	79.5 ± 2.7
PG 1237+132		
	46.4896	−36.1 ± 4.8
	46.5032	−31.6 ± 4.8
	54.5637	−31.3 ± 4.4
	54.5772	−36.4 ± 4.2
	55.6295	−33.5 ± 3.9
	55.6431	−35.5 ± 3.9
	56.5768	−29.1 ± 4.2
	56.5904	−34.4 ± 4.1
	57.5443	−50.1 ± 4.2
	57.5578	−44.5 ± 4.1
PG 1244+113		
	46.5409	61.9 ± 5.8
	46.5505	66.3 ± 6.1
	54.5907	−14.0 ± 6.9
	54.6003	−21.9 ± 5.9
PG 1248+164		
	46.5672	40.6 ± 1.8
	46.5875	44.5 ± 1.8
	56.5529	−63.8 ± 2.9
	56.5632	−69.8 ± 3.0
PG 1300+279		
	46.6051	52.0 ± 2.2
	46.6166	49.0 ± 2.2
	56.6042	−34.2 ± 2.5

Table 2 – *continued*

Name	HJD −2451600	Radial velocity (km s^{-1})
	56.6156	−43.4 ± 2.3
PG 1303+097		
	46.6356	28.9 ± 2.3
	46.6548	29.3 ± 2.6
	56.6651	36.1 ± 3.4
	57.5763	32.9 ± 2.5
	57.5954	27.0 ± 2.5
PG 1329+159		
	46.6683	−1.2 ± 2.8
	46.6720	−11.6 ± 2.7
	56.6277	16.2 ± 1.9
	56.6351	10.3 ± 2.0
PG 1417+257		
	46.6820	2.0 ± 1.5
	46.6945	1.6 ± 1.4
	51.5643	−7.3 ± 2.6
	51.5708	−9.4 ± 2.6
	55.6587	−1.6 ± 1.4
	55.6713	−2.8 ± 1.4
	56.6969	−5.0 ± 1.6
	56.7094	−1.2 ± 1.7
	57.6094	3.2 ± 2.5
	57.6158	0.7 ± 2.5
PG 1505+074		
	53.5699	7.4 ± 4.9
	53.5727	3.9 ± 4.7
	57.6275	−3.5 ± 1.9
	57.6380	5.6 ± 1.9
PG 1512+244		
	53.5782	−101.6 ± 3.4
	53.5837	−94.8 ± 3.2
	57.6469	−43.8 ± 2.9
	57.6525	−41.2 ± 3.0
PG 1553+273		
	53.5917	71.8 ± 2.0
	53.5987	71.4 ± 2.1
	56.6439	77.0 ± 1.9
	56.6509	79.5 ± 2.0
	57.6599	79.0 ± 1.8
	57.6670	75.1 ± 1.7
PG 1616+144		
	53.6083	−50.0 ± 4.9
	53.6160	−50.0 ± 4.8
	57.6805	−46.7 ± 2.4
	57.6958	−47.0 ± 2.3
PG 1619+522		
	46.7032	−70.1 ± 3.4
	46.7081	−75.4 ± 3.3
	51.5444	−67.4 ± 3.3
	51.5518	−68.0 ± 3.4
	53.6887	−31.9 ± 4.0
	53.6937	−40.1 ± 3.9
PG 1627+017		

Table 2 – *continued*

Name	HJD −2451600	Radial velocity (km s^{-1})
	53.6236	−125.0 ± 3.3
	53.6261	−126.9 ± 3.2
	54.6144	−66.7 ± 2.5
	54.6169	−69.0 ± 2.5
PG 1631+267		
	53.6559	−42.1 ± 0.6
	53.6677	−41.3 ± 0.6
PG 1632+088		
	53.6329	189.6 ± 1.2
	53.6398	191.0 ± 1.1
PG 1647+056		
	54.6305	−106.3 ± 3.0
	54.6521	−113.4 ± 3.1
PG 1653+131		
	54.6724	4.3 ± 2.3
	54.6872	7.4 ± 2.3
PG 1701+359		
	46.7176	−120.7 ± 1.5
	46.7259	−121.2 ± 1.5
	51.5771	−117.2 ± 2.5
	51.5822	−117.6 ± 2.3
	54.7222	−119.4 ± 1.5
	54.7304	−122.8 ± 1.5
	55.7250	−118.4 ± 1.4
	55.7333	−118.7 ± 1.4
	56.7198	−121.9 ± 1.6
	56.7281	−118.3 ± 1.6
PG 1710+490		
	46.7328	−56.6 ± 3.4
	46.7354	−59.3 ± 3.4
	51.5869	−52.8 ± 4.3
	51.5885	−51.8 ± 4.3
	51.6170	−49.4 ± 2.5
	51.6208	−49.4 ± 2.3
	53.7003	−49.3 ± 2.5
	53.7040	−54.5 ± 2.5
	54.7094	−60.4 ± 2.2
	54.7131	−58.9 ± 2.2
	55.7121	−55.8 ± 2.3
	55.7158	−61.7 ± 2.4
	56.7569	−54.9 ± 2.6
	56.7618	−47.4 ± 5.2
PG 1716+426		
	46.7446	−52.4 ± 2.1
	46.7552	−53.5 ± 2.2
	51.5972	58.3 ± 2.3
	51.6078	48.2 ± 2.4
	57.7333	−73.5 ± 2.0
	57.7481	−71.5 ± 1.9
PG 1722+286		
	51.7498	−47.5 ± 4.1
	51.7551	−38.9 ± 4.4
	53.7329	−33.2 ± 4.3
	53.7382	−40.3 ± 4.2
	57.7091	−37.2 ± 2.6
	57.7195	−35.6 ± 2.7
PG 1725+252		
	51.7613	−63.5 ± 6.1
	51.7629	−67.0 ± 9.1
	53.7578	38.0 ± 3.5
	53.7610	40.2 ± 4.2
	54.7494	−93.7 ± 1.6
	54.7554	−86.7 ± 1.8
PG 1743+477		
	53.7123	38.3 ± 2.1
	53.7220	28.7 ± 2.2
	55.6932	39.3 ± 1.8
	55.7029	45.3 ± 1.9
	56.7376	44.7 ± 2.1
	56.7474	50.2 ± 2.2

mean is the best estimate of the radial velocity of the star assuming this quantity is constant. We then calculate the χ^2 statistic for this 'model', i.e. the goodness of fit of a constant to the observed radial velocities. We can then compare the observed value of χ^2 with the distribution of χ^2 for the appropriate number of degrees of freedom. We then calculate the probability of obtaining the observed value of χ^2 or higher from random fluctuations of constant value, p. To allow for the systematic errors described above, we have added a 2 km s^{-1} external error in quadrature to all the radial velocity uncertainties prior to calculating these statistics. If we find $\log_{10}(p) < -4$ we consider this to be a detection of a binary. In our sample of 36 EHB stars, this results in a less than 0.4 per cent chance of random fluctuations producing one or more false detections.

3.4 Results

The observed values of χ^2 and $\log_{10}(p)$ and the number of measured radial velocities, N, are given for all the targets in our sample in Table 3. Stars that were observed but are not EHB stars are shown in parentheses. Stars that we consider to be binaries are denoted by displaying $\log_{10}(p)$ in bold type. In column 3 we give the maximum difference between the observed radial velocities, Δ. In column 6 (SLY98) we note whether Saffer et al. (1998) saw a marginal detection (2) or a positive detection (1) of a radial velocity shift or failed to detect any radial velocity shift (×). In column 7 (JP98) we note whether Jeffery & Pollacco (1998) saw spectral features resulting from a cool companion (Y) or failed to detect a companion (×). In column 8 (AWFBL98) we note whether the *BVRI* photometry of Allard et al. (1994) failed to detect a companion (×) or note the spectral type of the companion if it was detected. In column 8 (UT98) we note stars for which Ulla & Thejll (1998) did not detect any infrared excess resulting from a companion from their *JHK* photometry (×). Stars for which comments can be found in Section 4 are noted in column 9. There are 36 EHB stars in our sample, 21 of which are binaries. With the exception of PG 1716+426 and, perhaps, PG 0839+399, these are all new detections.

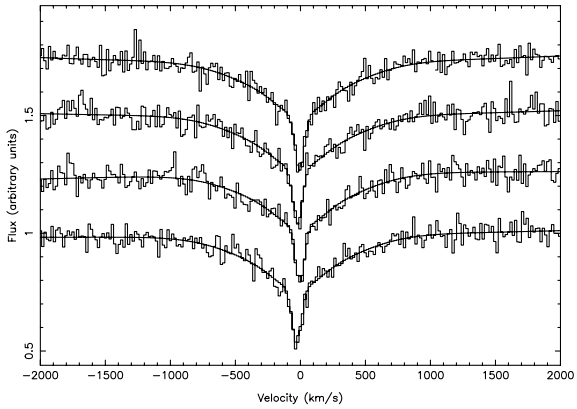

Figure 3. An example of the observed spectra and multiple Gaussian fits used to measure the radial velocities given in Table 2. The spectra of PG 1043+760 are shown plotted as histograms together with the model fits shown as thick lines. The spectra are normalized and offset by 0.25 units relative to one another. The wavelength is given as a velocity relative to the rest wavelength of Hα.

4 NOTES ON INDIVIDUAL OBJECTS

In this section we note previous results for our targets and any other remarkable or peculiar characteristics.

PG 0749+658. Late-type spectral features can be seen in the average spectrum of this star shown in Fig. 4.

PG 1018−047. There are weak spectral features arising from a late-type companion visible in our spectra.

PG 1039+219. This star in listed in Jeffery & Pollacco as Ton 1273.

PG 1040+234. Spectral features arising from the companion are seen in our blue spectra of this star, notably the G-band and Ca II H and K spectral lines, and some weak features can also be seen around Hα (Fig. 4).

PG 1047+003. This is a pulsating sdB variable star (Billères et al. 1997).

PG 1114+073. Saffer, Livio & Yungelson list this star as PG 1114+072.

PG 1631+267. This star has a bright G-type companion which dominates the spectrum around the Hα line so the radial velocities quoted here refer to the G-star companion to the sdB star, which we denote PG 1631+267 B.

PG 1701+359. Theissen et al. noted spectral features from a

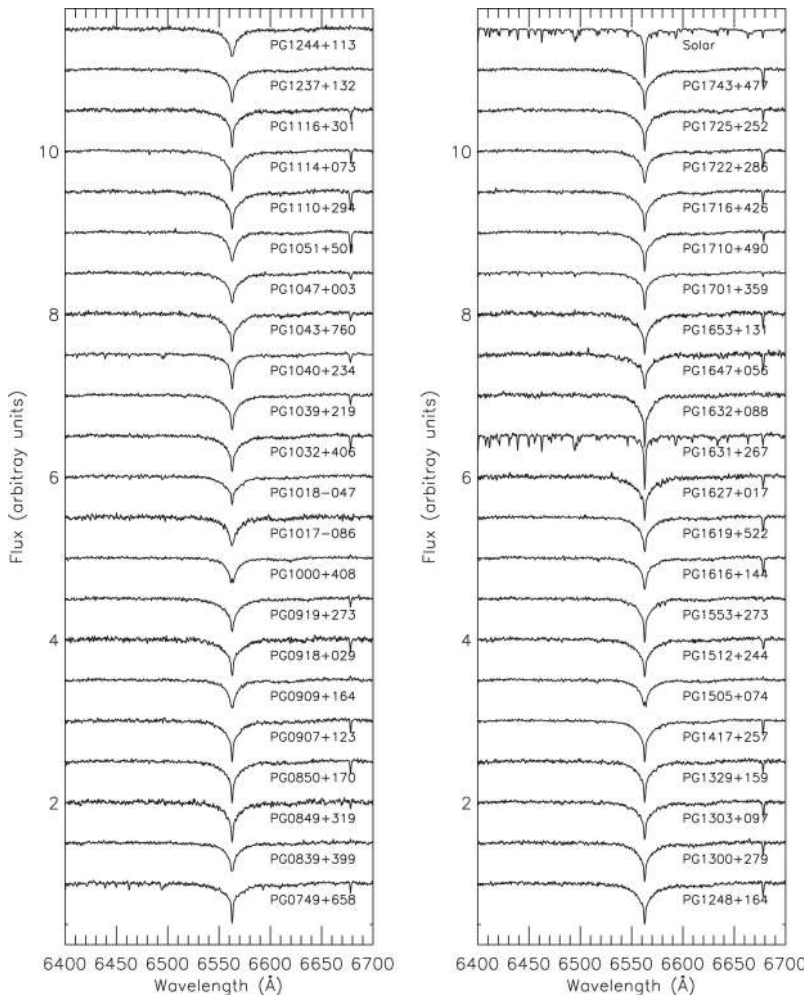

Figure 4. The average spectrum of each star. The spectra are normalized and offset by 0.5 units relative to one another. A spectrum of the twilight sky labelled 'Solar' is shown for comparison.

Table 3. Summary of our radial velocity measurements for subdwarf-B stars. See Section 3.4 for details.

Name	N	Δ(km s^{-1})	χ^2	$\log_{10}(p)$	SLY98	JP98	AWFBL94	UT98	Notes
PG 0749+658	10	17.6 ± 4.6	20.24	−1.78	×		K5.5		*
PG 0839+399	6	75.2 ± 6.9	172.21	**−34.61**	2	×			
PG 0849+319	4	44.5 ± 4.9	89.41	**−18.53**					
PG 0850+170	4	44.0 ± 2.7	220.23	**<− 45**		×			
PG 0907+123	6	66.2 ± 5.2	317.49	**<− 45**		×			
(PG 0909+164)	8	25.7 ± 8.6	14.73	−1.40					
PG 0918+029	4	81.3 ± 11.9	114.38	**−23.90**	×				
PG 0919+273	4	25.8 ± 5.0	30.92	**−6.05**	×				
(PG 1000+408)	10	37.8 ± 11.9	31.57	**−3.63**			×		
PG 1017−086	2	61.7 ± 9.6	38.16	**−9.19**					
PG 1018−047	8	17.7 ± 5.6	13.13	−1.16					*
PG 1032+406	4	38.4 ± 4.2	89.89	**−18.63**					
PG 1039+219	6	8.4 ± 4.2	5.06	−0.39		×			*
PG 1040+234	8	5.2 ± 3.4	2.35	−0.03		Y	K3.5		*
PG 1043+760	4	24.3 ± 4.6	30.08	**−5.88**					
PG 1047+003	6	13.0 ± 6.5	5.71	−0.47		×			*
(PG 1051+501)	6	9.1 ± 5.8	2.33	−0.10		×			
PG 1110+294	6	54.9 ± 9.5	156.96	**−31.36**					
PG 1114+073	8	6.2 ± 2.5	3.94	−0.10	×				*
PG 1116+301	4	171.9 ± 4.8	2203.13	**<− 45**					
PG 1237+132	10	21.0 ± 5.9	17.06	−1.32					
PG 1244+113	4	86.9 ± 8.5	161.99	**−34.17**		×			
PG 1248+164	4	114.3 ± 3.5	1195.15	**<− 45**					
PG 1300+279	4	95.5 ± 3.2	867.74	**<− 45**					
PG 1303+097	5	9.1 ± 4.2	4.16	−0.41					
PG 1329+159	4	27.9 ± 3.3	47.63	**−9.59**					
PG 1417+257	10	12.6 ± 3.7	17.19	−1.34					
(PG 1505+074)	4	10.9 ± 5.3	6.75	−1.10					
PG 1512+244	4	60.4 ± 4.5	224.53	**<− 45**				×	
(PG 1553+273)	6	8.1 ± 2.9	7.73	−0.76					
PG 1616+144	4	3.3 ± 5.5	0.53	−0.04					
PG 1619+522	6	43.5 ± 5.2	90.70	**−17.32**					
PG 1627+017	4	60.2 ± 4.0	273.94	**<− 45**			×		
(PG 1631+267 B)	2	0.9 ± 0.8	0.09	−0.12					*
(PG 1632+088)	2	1.3 ± 1.6	0.16	−0.16					
PG 1647+056	2	7.1 ± 4.3	1.90	−0.78			K8		
PG 1653+131	2	3.0 ± 3.2	0.50	−0.32			×		
PG 1701+359	10	5.6 ± 2.9	4.75	−0.07			K6.5		*
PG 1710+490	14	14.2 ± 5.7	23.00	−1.38					
PG 1716+426	6	131.8 ± 3.1	2040.05	**<− 45**	1				*
PG 1722+286	6	14.4 ± 5.9	6.29	−0.55					
PG 1725+252	6	133.8 ± 4.5	1326.41	**<− 45**			×		
PG 1743+477	6	21.5 ± 3.1	32.10	**−5.25**					

cool star in their spectra. Spectral features from a cool star are also visible in our spectra around the Hα line.

PG 1716+426. Geffert (1998) considers the galactic orbit of this star based on the *Hipparcos* astrometry and a radial velocity measurement of $-10.6 \pm 30\,\mathrm{km\,s^{-1}}$. Clearly, this calculation needs to be revised.

5 DISCUSSION

5.1 Estimating the binary fraction

The probability of detecting N_B binaries in a sample of N stars which have a binary fraction of f is

$$\frac{N!}{(N-N_\mathrm{B})!N_\mathrm{B}!}(\bar{d}f)^{N_\mathrm{B}}(1-\bar{d}f)^{N-N_\mathrm{B}},$$

where $\bar{d}$ is the fraction of all binaries detected by the survey averaged over all orbital periods. For our survey, $N_\mathrm{B} = 21$ and $N = 36$. We can set a lower limit to f by assuming $\bar{d} = 1$, i.e. the lower limit to f is set by assuming we have detected all the binaries in our sample. In this case we expect that the lower limit to the binary fraction will be about 21/33 = 58.3 per cent. In fact, the distribution of f calculated with the expression above with $\bar{d} = 1$ is approximately Gaussian with a maximum at $f = 0.60$ and a standard deviation of 0.08, i.e. the absolute lower limit to f from our survey is 60 ± 8 per cent.

We calculated the fraction of all binaries of a given orbital period, P, detected by our survey, d, as follows. We assume that the EHB star and its companion both have a mass of $0.5\,\mathrm{M}_\odot$. We can then calculate the orbital speed of the EHB star, V_orb, assuming a circular orbit. We assume the that orbits are circular because a common envelope phase will quickly reduce the eccentricity of an orbit and no post-common envelope systems are observed to have any appreciable eccentricity. For a given star for which we have N_obs radial velocity measurements we can then use the actual dates of observation, T_j, $j = 1 \ldots N_\mathrm{obs}$ to calculate radial velocities for a hypothetical binary with an edge-on orbit from $V_\mathrm{orb}\sin(\phi_i)$, where $\phi = (T_j - T_0)/P$. These values are used to calculate the value of χ^2 for this hypothetical binary, χ^2_max, using the actual radial velocity uncertainties for the N_obs observations given in Table 2 including $2\,\mathrm{km\,s^{-1}}$ additional systematic uncertainty. The calculation is repeated for 50 values of the T_0 and the average value of

$\chi^2_{\rm max}$ is taken. We can then compare the value of $\chi^2_{\rm max}$ for this hypothetical binary to the value of χ^2 required to exactly satisfy our detection criterion, $\chi^2_{\rm crit}$. If $\chi^2_{\rm max} < \chi^2_{\rm crit}$ then no binaries with that orbital period, mass and eccentricity will be detected by our observations.[1] Otherwise, we can calculate the projected orbital velocity for which $\chi^2_{\rm max} = \chi^2_{\rm crit}$, $K_{\rm crit} = V_{\rm orb} \sin i$ for some orbital inclination i. For randomly oriented orbits, i is distributed as $\cos i$ so the fraction of binaries detected for this combination of observations, period, mass etc. is simply $d = \sqrt{1 - (K_{\rm crit}/V_{\rm orb})^2}$. We have calculated this detection efficiency for 20 000 orbital periods distributed uniformly in $\log_{10}(P)$ over the range $-1.5 \leq \log_{10}(P/{\rm d}) \leq 2$ for every EHB star we observed and used these values to calculate the average detection efficiency for stars in our sample, d. The results are shown in Fig. 5, where the value of d has been binned into 400 groups of 50 periods.

To calculate the binary fraction of EHB stars, we need to know $\bar{d}$, the weighted mean of d over the period distribution of EHB binaries. Unfortunately, the period distribution of EHB binaries is very poorly known. The existing observational data for EHB stars with measured orbital periods is rather scarce, but is summarized in Table 4 and is also shown in Fig. 5. We are not aware of any reliable predictions for the orbital period distribution based on models of the evolution of EHB stars. From the size of the radial velocity shifts given in Table 3 we can set an upper limit to the orbital period of the binaries we have found. These are typically tens of days, so the actual orbital periods are likely to be $\lesssim$10 d.[2]

In the absence of any good determination of the orbital period distribution of binary EHB stars for longer orbital periods, we consider the binary fraction for short orbital period binaries only ($P \lesssim 10$ d). We can see from Fig. 5 that any reasonable period distribution will give a mean detection efficiency over $-1.5 \leq \log_{10}(P/{\rm d}) \leq 1$ of about 85 per cent. For example, the unweighted average over this range of $\log_{10}(P)$ is 86.6 per cent, which implies a binary fraction of 69 ± 9 per cent. If, for the sake of argument, we assume a distribution for $\log_{10}(P)$ which is a Gaussian function with a mean of $\log_{10}(P/{\rm d}) = 0$ and a full width at half-maximum of $\log_{10}(P/{\rm d}) = 2$, the mean detection efficiency over $-1.5 \leq \log_{10}(P/{\rm d}) \leq 1$ is 84.7 per cent so we obtain a binary fraction of 70 ± 9 per cent. If we change the mean of the Gaussian function to $\log_{10}(P/{\rm d}) = -1$, the mean detection efficiency over the same range of $\log_{10}(P)$ is 91.1 per cent and the binary fraction is 65 ± 9 per cent. These are all ad hoc assumptions for the period distribution of binary EHB stars, but they do show that the fraction of EHB stars that are short-period binaries is about 2/3 for any reasonable period distribution.

This calculation is also insensitive to the assumed mass ratios of the binaries. If we assume the companions have a mass of 1 $M_\odot$, the lower limits to the binary fraction we derive are reduced by 1–2 per cent. The mean companion mass is unlikely to be larger than 1 $M_\odot$ because a main-sequence or subgiant star of this mass would be easily visible in the spectrum and the upper limit to the white dwarf companion mass is, of course, the Chandrasekhar mass of 1.4 $M_\odot$. We do not expect there to be large numbers of neutron star or black hole companions to EHB stars. If the companions have a lower mean mass, our detection efficiency would be lower than the value calculated, so the minimum binary fraction we would derive would be higher. In summary, the minimum binary fraction implied by our observations is about 69 ± 9 per cent and this result is not strongly dependent on the assumed distributions of period or mass ratios for short period EHB binaries.

Of course, if there are also binary EHB stars with longer periods, these would not be detected as frequently by our survey as the shorter period binaries, so the binary fraction may be much higher than 2/3. At some point the orbital period is too long for the binary to be relevant to this discussion. The binaries of interest are those for which the orbital separation now is less than the size of a red giant star near the tip of the red giant branch (RGB). In these cases, we can say that the companion has influenced the formation process of the EHB star. The radii of red giants near the tip of the RGB are $\approx$100 $R_\odot$, which corresponds to orbital periods of a hundred days or more. We can see from Fig. 5 that most binary EHB stars with orbital periods of tens of days would be missed by our survey. Therefore, if about 1/3 of EHB stars are binaries with orbital periods 10 d $\lesssim P \lesssim$ 100 d, then our results are consistent with all EHB stars being formed through interactions with a companion star.

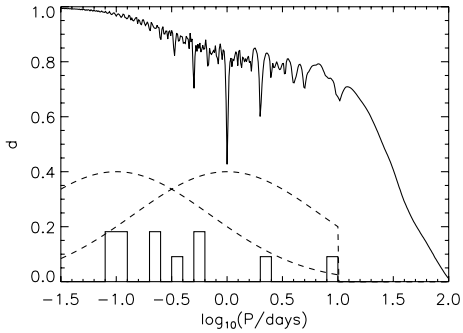

Figure 5. The fraction of binaries detected by our survey, d, as a function of the orbital period, P (thick line). The Gaussian weighting functions described in the text (dashed lines) and the distribution of orbital periods for known EHB binaries given in Table 4 (histogram) are also shown.

Table 4. Measured orbital periods and companion masses, M_2 for binary EHB stars. The lower limits to the companion masses have been calculated from the projected orbital velocity assuming a mass for the EHB star of 0.5 $M_\odot$. White dwarf companions are denoted 'WD', otherwise the spectral type of the companion, if known, is given.

Name	Period (days)	M_2 ($M_\odot$)	Companion type	Ref.
KPD 0422+5421	0.090	0.53	WD	2
KPD 1930+2752	0.095	0.97	WD	7
PG 1336−018	0.101	0.15	M5	5
HW Vir	0.117	0.14	dM	4
PG 1432+159	0.225	>0.29	WD	1
PG 2345+318	0.241	>0.38	WD	1
PG 1101+249	0.354	>0.42	WD	1
PG 0101+039	0.570	>0.37	WD	1
PG 1247+553	0.599	>0.09	–	3
PG 1538+269	2.501	0.6	WD	6
PG 0940+068	8.33	>0.63	–	3

1 Moran et al. (1999); 2 Orosz & Wade (1999); 3 Maxted et al. (2000a); 4 Wood & Saffer (1999); 5 Kilkenny et al. (1998); 6 Ritter & Kolb (1998); 7 Maxted et al. (2000b).

[1] This is not strictly true. Adding random fluctuations to the $V_{\rm orb}\sin(\phi_i)$ values can result in detections in cases where $\chi^2_{\rm max}$ is only slightly less then $\chi^2_{\rm crit}$. Similarly, noise can prevent some detections when $\chi^2_{\rm max}$ is slightly greater than $\chi^2_{\rm crit}$. The overall effect is negligible when the detection effeciency is averaged over a wide range of orbital periods as we have done.

[2] Observations to determine the actual orbital periods are being undertaken at the time of writing.

5.2 Other surveys

We note that there is no significant radial velocity shift in any of the stars for which there is evidence of a cool companion (PG 0749+658, 1018−047, 1040+234, 1647+056 and 1701+359). There is a bias in our sample in the sense that the orbital separation of a binary with two 0.5-$M_{\odot}$ stars may be too small to contain a main-sequence or subgiant K star for the shorter orbital periods where our survey has the greatest sensitivity. However, our observations are still quite sensitive to periods of a day or more, at least for PG 1040+234 and 1701+359. The orbital separation for an orbital period of a few days is several solar radii. This may suggest that there is a real trend for EHB stars with K-type companions to have long orbital periods.

Of the six stars observed by Saffer, Livio & Yungelson (1998), hereafter SLY, which also appear in our sample, we find four to be binaries. Two of these binaries were not detected by SLY (PG 0918+029 and 0919+273), one was noted as a marginal detection (PG 0839+399) and one as a positive detection (PG 1716+426). The shifts seen by us for PG 0918+029 suggest that it is at the limit of detection for the method employed by SLY. Curiously, the shift we observed for PG 0839+399, for which SLY note a marginal detection, is smaller than that of PG 0918+029, which suggests that our observations have not yet sampled the full range of radial velocity shifts for this star. The shift of only 25.8 km s^{-1} we measured for PG 0919+273 would not have been seen by SLY.

5.3 Post-EHB stars

Of the stars observed which we have excluded from this discussion, five appear to be stars that have evolved away from the extreme horizontal branch. One of these post-EHB stars is a good candidate to be a binary from our data (PG 1000+408). Observations by Green (private communication) have shown that PG 1000+408 is indeed a binary with an orbital period near 1 d. There are too few stars in this subsample to derive useful limits on the binary fraction of these stars, though this would obviously be an interesting number because we would expect it to be similar to the binary fraction for normal EHB stars if the two groups of stars are related as we have suggested.

5.4 Selection effects

One advantage of choosing objects from the PG survey is that we were able to choose brighter stars based on their photographic magnitudes without introducing a bias in our sample towards short-period binaries. This is because the majority of the short-period binaries have white dwarf or K/M dwarf companions, both of which contribute a negligible amount of light in the blue region of the spectrum on which the PG survey is based. One type of binary we are biased against are those containing brighter F/G-type companions. Most of these binaries were excluded from the PG survey because stars showing the Ca II K line were assumed to be main-sequence subdwarfs with normal colours which appeared bluer owing to the substantial uncertainty in the photographic photometry on which survey is based (Green et al. 1986). In fact, a substantial fraction of these stars may be sdB stars with F/G-type companions (Kilkenny et al. 1997). Some sdB stars with an F/G-type companion are included in the PG survey, e.g. PG 1631+267. Although we cannot measure the radial velocities of the sdB star from the Hα line in these cases, we can measure the radial velocities of the F/G star from its Hα line, if it dominates at the wavelength, or from the many other absorption lines should the Hα line be a blend of the sdB star and the F/G star Hα line. In fact, these radial velocities are preferable to the sdB velocities in some ways as they are more accurate and we can estimate the mass of the companion star from its spectral type.

5.5 Triple stars

The effect of the selection criterion against F/G companion stars applied to the PG survey is difficult to judge without knowing the actual fraction of sdB stars with F/G-type companions that have been 'lost' from the survey. We note that this effect also biases the results of Allard et al. (1994), Ferguson et al. (1984) and Jeffery & Pollacco (1998). Nevertheless, these authors still find 1/2–2/3 of their sample have cool companion stars. We have already noted that the EHB stars we have observed to be binaries do not have cool companions. The total binary make-up is then 2/3 short-period sdB stars without cool companions plus 1/2–2/3 with cool companions in the PG survey plus the 'lost binaries' with cool companions excluded from the PG survey minus a small fraction of short-period sdB stars with cool companions. This number is clearly greater than 1, an apparent paradox which is easily explained by some of the sdB stars being triple stars, i.e. short-period sdB stars with M-dwarf or white dwarf companions and a distant F/G-type cool companion that was not involved with the evolution of the inner pair.

6 CONCLUSION

We have measured 205 precise radial velocities for 36 extreme horizontal branch stars to look for variability arising from a close binary companion. We found that 21 of our stars are positively identified as short-period binaries. All but one or two of these are new identifications. We conclude that at least 2/3 of all EHB stars are short-period binaries. The orbital separations of these binaries are much less than the size of the star during the red giant phase which almost certainly preceded its emergence as an EHB star. We conclude that some kind of interaction with a binary companion, perhaps in a common envelope phase, is fundamental to the formation process for the majority of EHB stars.

ACKNOWLEDGMENTS

PFLM was supported by a PPARC post-doctoral grant. The Isaac Newton Telescope is operated on the island of La Palma by the Isaac Newton Group in the Spanish Observatorio del Roque de los Muchachos of the Instituto de Astrofisica de Canarias. PFLM thanks E.M. Green and R.A. Saffer for many informative discussions on the subject of sdB stars. We thank Rex Saffer for providing us with his results for sdB stars. We thank Martin Altmann for his spectrum of PG 0907+123.

REFERENCES

Allard F., Wesemael F., Fontaine G., Bergeron P., Lamontagne R., 1994, AJ, 107, 1565

Bergeron P., Fontaine G., Lacombe P., Wesemael F., Crawford D. L., Jakobsen A. M., 1984, AJ, 89, 374

Bergeron P., Saffer R. A., Liebert J., 1992, ApJ, 394, 228

Billéres M., Fontaine G., Brassard P., Charpinet S., Liebert J., Saffer R. A., Vauclair G., 1997, ApJ, 487, L81

D'Cruz N. L., Dorman B., Rood R. T., O'Connell R. W., 1996, ApJ, 466, 359
Dorman B., Rood R. T., O'Connell R. W., 1993, ApJ, 419, 596
Duquennoy A., Mayor M., 1991, A&A, 248, 485
Ferguson D. H., Green R. F., Leibert J., 1984, ApJ, 287, 320
Geffert M., 1998, A&A, 340, 305
Green R. F., Schmidt M., Liebert J., 1986, ApJS, 61, 305
Heber U., 1986, A&A, 155, 33
Heber U., Reid I. N., Werner K., 2000, A&A, 363, 198
Iben I., Livio M., 1993, PASP, 105, 1373
Jeffery C. S., Pollacco D. L., 1998, MNRAS, 298, 179
Kilkenny D., O'Donoghue D., Koen C., Stobie R. S., Chen A., 1997, MNRAS, 287, 867
Kilkenny D., O'Donoghue D., Koen C., Lynas-Gray A. E., van Wyk F., 1998, MNRAS, 296, 329
Koen C., Orosz J. A., Wade R. A., 1998, MNRAS, 300, 695
Marsh T. R., 1989, PASP, 101, 1032
Maxted P. F. L., Marsh T. R., 1999, MNRAS, 307, 122
Maxted P. F. L., Moran C. K. J., Marsh T. R., Gatti A. A., 2000a, MNRAS, 311, 877
Maxted P. F. L., Marsh T. R., North R. C., 2000b, MNRAS, 317, L41
Mengel J. G., Norris J., Gross P. G., 1976, ApJ, 204, 488
Moehler S., Richtler T., de Boer K. S., Dettmar R. J., Heber U., 1990, A&AS, 86, 53
Moran C., Maxted P., Marsh T. R., Saffer R. A., Livio M., 1999, MNRAS, 304, 535
Napiwotzki R., 1997, A&A, 322, 256
O'Donoghue D., Koen C., Lynas-Gray A. E., Kilkenny D., van Wyk F., 1998, MNRAS, 296, 306
Orosz J. A., Wade R. A., 1999, MNRAS, 310, 773
Ritter H., Kolb U., 1998, A&AS, 129, 83
Saffer R. A., Bergeron P., Koester D., Liebert J., 1994, ApJ, 432, 351
Saffer R. A., Livio M., Yungelson L. R., 1998, ApJ, 502, 394, (SLY)
Theissen A., Moehler S., Heber U., de Boer K. S., 1993, A&A, 273, 524
Ulla A., Thejll P., 1998, A&AS, 132, 1
Wesemael F., Fontaine G., Bergeron P., Lamontagne R., Green R. F., 1992, AJ, 104, 203
Wood J. H., Saffer R., 1999, MNRAS, 305, 820

This paper has been typeset from a TEX/LATEX file prepared by the author.